ON THE KINETICS OF ALH3 DECOMPOSITION AND THE SUBSEQUENT AL OXIDATION

Eisenreich N., Keßler A., Koleczko A., Weiser V.
Fraunhofer-Institut für Chemische Technologie (ICT), J-v-Fraunhoferstr. 7, D76327 Pfinztal, Germany, ne@ict.fraunhofer.de

ABSTRACT

Metal hydrides are used for hydrogen storage. AlH_3 shows a capacity of about 10wt% and the hydrogen is split-off in the temperature interval of 400-500K. On dehydrogenation a nano-structured Al material emerges which is oxidized on air access up to 25%, forming a 3-4 nm alumina layer. The heat released from this Al oxidation induces a high risk to this type of hydrogen storage if the containment might be destroyed, accidentally. The kinetics of the dehydrogenation and the subsequent oxidation is investigated by methods of thermal analysis. A reaction scheme is confirmed which consists of a starting Avrami-Erofeev mechanism followed by formal 1st order oxidation. The kinetic parameters are evaluated and can be used to calculate the reaction progress together with heat of reaction of Al oxidation.

1.0 INTRODUCTION

Current investigations of metallic hydrides aim at twofold applications. Aluminium hydride (alane) might be used as a component in energetic materials, especially for rocket propellant charges [1-10]. The thermal decomposition under vacuum and inert atmospheres is of high interest for its utilisation for hydrogen storage [11-15]. Stability problems arising on utilization of technical grade materials prevented past application. This situation has changed as stabilized material is currently available on large scale, as was proven in detail by thermo-analytical investigations [10, 16, 17].

The hydrogen split-off mechanism and its kinetics was investigated to analyse the storage and aging effects of the stabilized material [10 -14]. It is mainly important for applications for hydrogen storage. Details of the hydrogen desorption mechanism are reported in several papers [4, 9, 10-15, 19-25]. An Avrami-Erofeev (A-E) [10-14, 23-25] mechanism is generally assumed for this process. The alane crystals are converted to porous Al particles of the same shape.. The activation energy was found to be close to 100 kJ. However, it is difficult to understand that the current assumption that nucleation and crystal growth (A-E) should be the rate controlling step of the thermally stimulated loss of hydrogen. X-ray diffraction shows the AlH_3 lattice to be observable throughout the decomposition [13-15, 24, 25]. Ismail and Hawkins [10] introduced a 2 step process and derive kinetic parameters to explain storage tests. When alane splits off the hydrogen in a storage and release cycle, the resulting neat Al is nano-structured. Already the subsequent passivation reaction converts up to 25% Al to Al_2O_3 when exposed to air. The related released heat would increase the temperature of the material to more than 1000K and might initiate an explosion [24, 25] and induce a serious safety problem on destruction of the containments. The electro-exploded aluminium ALEX contains a the passivation layer consisting of 20-25% alumina [26- 32] and can therefore be compared to the nano-structured Al on alane decomposition. The recrystallization depends on the heating rate of alane and via the crystallite size of the resulting Al heating rate depending surface areas are accessible to passivation (oxidation of a thin metal layer at the particle surface) and therefore generates the related heat of oxidation. The subsequent oxidation process includes further reaction steps by which the residual nano-/micro-porous aluminium structures are converted to alumina [26-31]. AlH_3 dehydrogenation should therefore avoid any risk of air access

In this paper, the hydrogen split-off is re-investigated to evaluate the kinetic parameters of the passivation reaction in 2 consecutive steps. In ref. [24, 25] the passivation reaction is described only qualitatively. However, there exist no kinetic data are published, only results of a Charge Molecular-Dynamics Simulations, but they are needed to estimate the dynamics of an auto-thermal explosion.

2.0 EXPERIMENTAL

The investigated alane was a poly-crystalline powder of a particle size of 10-20 µm including also a fraction of a size of 1-2 µm. The used AlH_3 is stable since various approaches were successful [16, 17] and the material correspond to that used for rocket propellant applications [1, 2]. The average density, as measured by pycnometery, was 1.477 g/cm^3. Pictures of Scanning Electron Microscopy showed that the particles consisted of round edged α-AlH_3 polyhedra as cubes, cubic octahedron and hexagonal prisms, as well as particles composed of these shapes (see Fig.1).

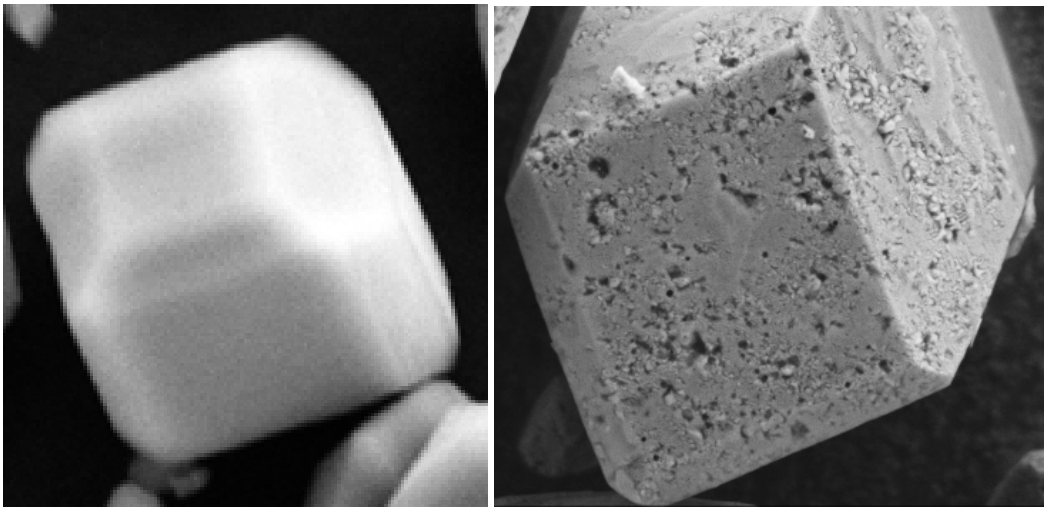

Figure 1: left hand side: SEM pictures of alane, right hand side: Al particle after alane dehydrogenation, edge length of particles is 20 µm

X-Ray diffraction confirmed the hexagonal unit cell and lattice parameter a 4.446 Å at 333 K and 4.447 Å, parameter c 11.81 Å at 433 K immediately before decomposition [24, 25]. A detailed X-Ray study on alane dehydrogenation is published by Maehlen et al [14]. It showed that Al emerges with small amounts of Al_2O_3 between 420 and 480 K. The resulting Al is oxidized to α- Al_2O_3 above 800 K. The TG and DSC experiments were conducted with a Netzsch Thermal Analyzer. The masses of investigated samples were between 3 and 6 mg on decomposition in Ar and 1 mg on oxidation in air with heating rates between 0.5 to 50 K/min. A qualitative discussion of the TG and DSC-curves for both case in argon and air occurred already a in the earlier paper [24, 25]. However, the thermo-analytical oxidation results in this paper were achieved with the sample subjected to a flow of air and not with the static air. The kinetic parameters are evaluated. The dehydrogenation and oxidation strongly overlap in the TG and DSC curves, the endothermic dehydrogenation being not clearly separated from the subsequent oxidation. To summarize earlier results alane dehydrates in inert atmospheres or vacuum between 400 and 500 K on heating [1-25]. The weight loss is between 9.0 to 9.9% whereas 10.1% might be expected in maximum.

After the dehydrogenation the resulting Al-cubes (prisms and octahedrons) exhibit a nano-micro-porous structure (see Fig 1) which enable the access of air to the Al-crystallites in the interior of these polyhedral particles [22-26]. As consequence of air access a passivation occurs forming a 3-4 nm layer as usual for Al and further heating in air initiates the oxidation in 2 steps as typical for sub-micron Al particles [26-28]. These effects are illustrated by Fig. 2. In Fig. 2 the heating of alane starts at room temperature under an inert atmosphere and splits-off hydrogen between 420 and 450 K, is then cooled down to room temperature, where a flow of air generates passivation of the resulting Al. It is then reheated under a flow of air where the Al undergoes a first oxidation step between 650 and 900 K forming an oxide layer of about 8-10 nm on the Al crystallites (see ref. [26-28]). The diffusion controlled reaction completes the Al oxidation above 1000 K. When heating alane directly in air starting from room temperature, the passivation overlaps the dehydrogenation step strongly. The weight increase (oxidation) depends on the heating rate which turns out to be lower with higher heating rates (Fig. 3). This trend is evident,

however the quantitative values scatter strongly. The subsequent oxidation at 800 K, which depends on the Al particle size, is related to this value and leads to a higher step if the weight increase in the passivation reaction is also higher. The weight increase is e.g. 22%, 9% and 4% in the curves of Fig. 3 which shows these reaction steps. A weight increase of 22% corresponds to a conversion of 25% Al to Al_2O_3. The DSC-curves (Fig. 4) correspond to the exothermic oxidations (31 kJ/g) mainly, the endothermic dehydrogenation (0.33 kJ/g [12, 13]) is hardly seen (below in the analysis) because the heat of reaction is small

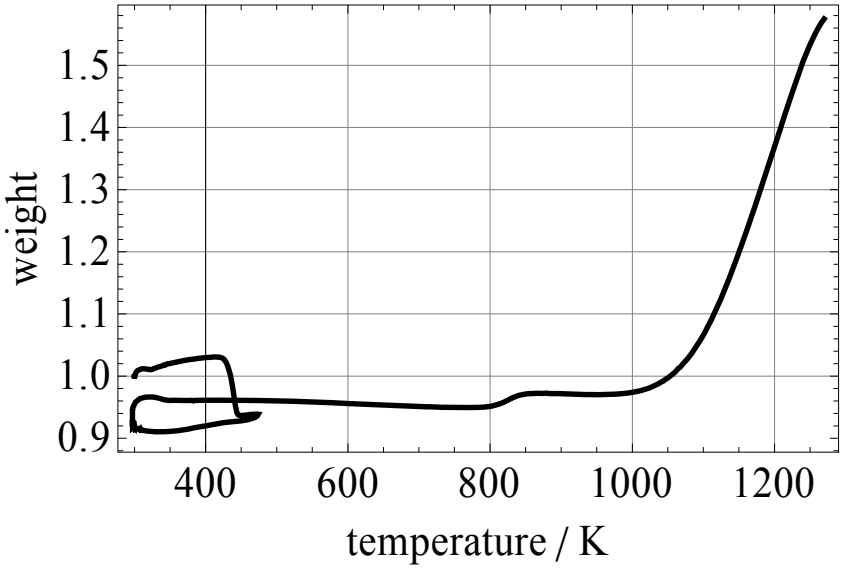

Figure 2: TG-curve heated (2 K/min) in an inert Ar-atmosphere till 480K initiating dehydrogenation, then cooled down to 50 K with entrainment causing passivation and subsequent heating to 1300 K (5 K/min) with two steps of oxidation at 850 K and 1100 K

compared to that of the oxidation. Fig. 5 shows the overlap of the dehydrogenation and passivation in detail for both the TG and DSC curves.

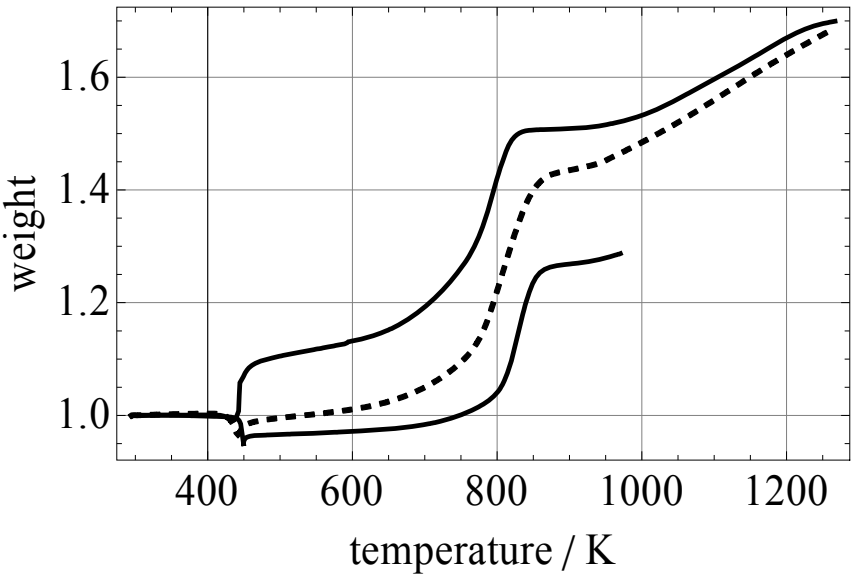

Figure 3: TG-curves (2 K/min, 5 K/min and 10 K/min) of AlH_3 heated in air with overlapping of dehydrogenation above 430K with the passivation reaction (oxidation of a 3-4 nm layer of resulting Al) with sub-sequent oxidation of resulting Al in 2 steps, higher heating rates shift reactions to occur at higher temperatures

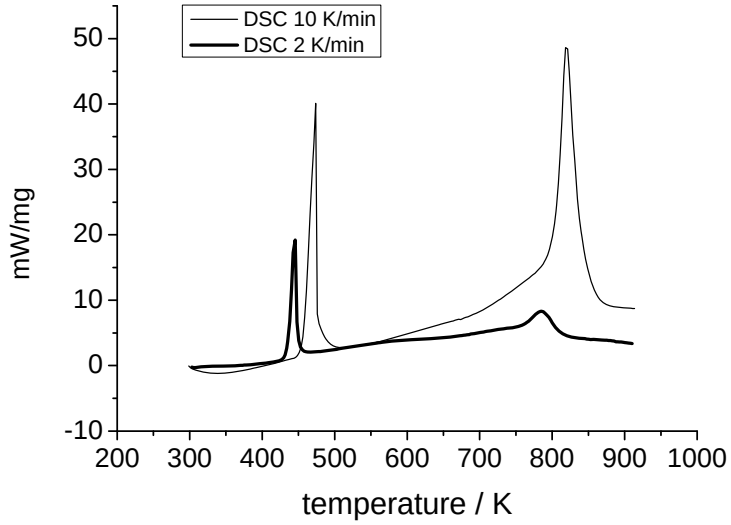

Figure 4: DSC-curves (2 and 10 K/min) of AlH_3 in air with overlap of dehydrogenation above 430 K and the highly exothermic passivation reaction (3-4 nm layer of Al) with sub-sequent highly exothermic oxidation of resulting Al in a step between 650 and 900 K, higher heating rates shift reactions to occur at higher temperatures

3.0 KINETIC EVALUATION

The reaction scheme for the decomposition and oxidation was already described earlier [24, 25]. It proceeds as follows: AlH_3 => Al => Al-crystallites + O2 => Al-crystallites with alumina passivation layer whereas the crystal growth and the oxidation are competing reactions, because the growths of crystal stops, once the surface is passivated. It is however discussed that the re-crystallization process would be the rate determining step [10, 11, 14] or at least be a parallel step. The strong overlap of passivation with dehydrogenation might be

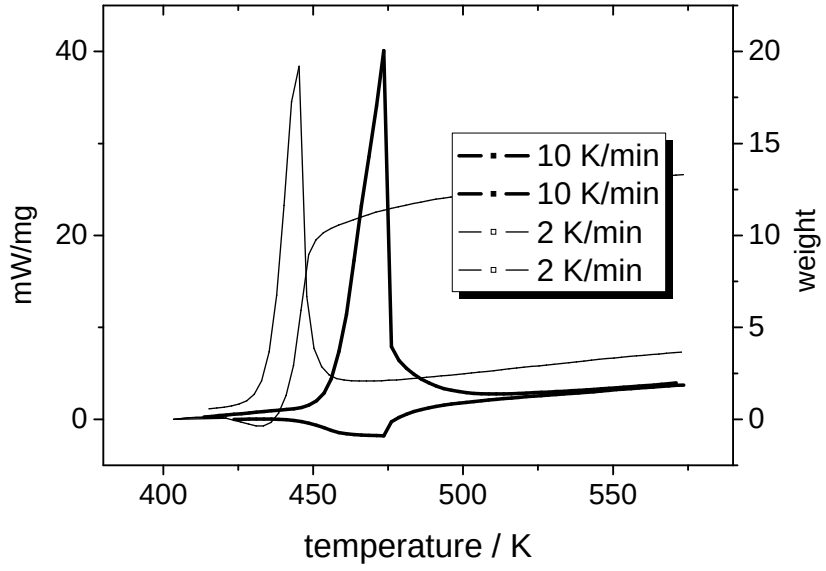

Figure 5: TG- and DSC-curve of the temperature region of dehydrogenation of AlH_3 and the subsequent passivation of the resulting Al.

consistent with this assumption. At lower temperatures a (at lower heating rates the dehydrogenation occurs at lower temperatures) the resulting Al crystallites are smaller and their passivation occurs shortly after dehydrogenation and remain therefore smaller at a size of the ALEX particles. The amount of the alumina of the passivation layer is higher due to larger crystallite surfaces. At higher heating rates the dehydrogenation takes place at higher temperatures forming bigger Al crystallites and therefore lower amounts of alumina in the passivation layer. Those bigger particles convert less Al in the step between 650 and 900 K as in this step a surface layer of 8-10 nm of alumina is formed [26-28]. This model is formulated as consecutive reaction steps with a linear heating rate A, the Arrhenius rate constants k(Z,E,T)=Z exp(-E/ RT), a Z pre-exponential [1/s] and an E activation energy [kJ/mole], the gas constant R and T the temperature [K]:

$$k(Z,E,T) = Ze^{-\frac{E}{RT}}; S(E,T) = \int e^{-\frac{E}{RT}} dT = Te^{-\frac{E}{RT}} \sum_{n=1}^{N} n!(-1)^{n-1} \left(\frac{RT}{E}\right)^n \qquad (1)$$

The partially successful modelling by an A-E reaction mechanism (below: n exponent of A-E mechanism, n≠1) might support the influence of crystallisation. It is also assumed here, but there is no indication in the thermo-analytical curves to need 2 A-E mechanisms as consecutive steps (see [10]), as also proved below by the acceptable agreement of the models with data, for

$$\begin{aligned}
\frac{d[AlH_3]}{dT} &= -n\frac{k_1(Z,E,T)}{A}[AlH_3](-\ln[AlH_3])^{\frac{n-1}{n}} \\
\frac{d[Al]}{dT} &= \frac{d[AlH_3]}{dt} - \frac{k_{2,cryst}(Z,E,T)}{A} f_{cryst}([Al]) - \frac{k_{3,oxid}(Z,E,T)}{A} f([Al]) \qquad (2) \\
\frac{d[Al_2O_3]}{dT} &= \frac{k_{3,oxid}(Z,E,T)}{A} f([Al])
\end{aligned}$$

This set of equations can be solved by integrals, for simplicity it is assumed that 1st order reactions f(c) occur in the 2nd steps. Oxidation and crystallization are assumed to be competing reactions. This means that the crystal growth stops if it is surrounded by a passivation layer, at least partially:

$$[AlH_3] = e^{-(\frac{Z}{A}S(E,T))^n} \qquad (3)$$

$$\begin{aligned}
[Al] &= ne^{-\frac{Z_2}{A}S_2(E_2T)} \int_0^T k_1(u)\left(\frac{Z_1}{A}S_1(E_1,u)\right)^{n-1} e^{\frac{Z_2}{A}S\ (E_2,u)-(\frac{Z_1}{A}S_1(E_1u))^n} du \\
[Al]_{cryst} &= \int_0^T k_2(u)[Al](u)du \qquad (4) \\
[Al_2O_3] &= \int_0^T k_4(u)[Al](u)du
\end{aligned}$$

The main indication of crystallisation might be assigned to the result that the increase of weight directly after decomposition depends on the heating rate. At lower heating rates < 2K/min the weight increases to more than 110% (related to 100% alane, 22% related to the resulting Al) and only to 102% with higher heating rates (50 K/min). Assuming that formed Al crystallites are covered by an oxide layer of about 3 nm thickness one can conclude that at higher heating rates bigger crystallites are generated which in total generate less passivation oxide. However, the reproducibility was not good enough to enable an evaluation of the kinetics by a least squares fit. Therefore this crystallisation reaction is only estimated with respect to obtain kinetic parameters. If all reactants are

normalised to 1 and 0 this does not interfere with the evaluation of the decomposition and oxidation reaction. Thermo-analytical curves are constructed from the set of equations (3) and (4) by:

TG curves with W the weight:

$$W_{dehyd}[T] = a_1 [AlH_3] \quad (5)$$

$$W_{oxi}[T] = a_1 [AlH_3] + a_2 [Al_2O_3] \quad (6)$$

and the DSC curve y:

$$y_{dehyd}[T] = Q_1 \, d[AlH_3] \, dT \quad (7)$$

$$y_{DSC}[T] = Q_1 \, d[AlH_3]/dT + p \, Q_2 \, d[Al]/dT \quad (8)$$

a_1, a_2 and p are parameter, which are used to normalize the selected parts of curves to 1 and 0 and to specify the proportion of material oxidized. Q_1 and Q_2 are the heats of reaction (kJ) of AlH_3 dehydrogenation and Al oxidation. $Q_2 >> -Q_1$, therefore in the DSC curves show only a deformation and not a negative dip in the curves prior to oxidation.

4.0 DATA EVALUATION FOR KINETIC PARAMETERS

The aim of this paper is to get kinetic data for the passivation of Al, although the simplest approach for the oxidation reaction is used. Despite a detailed evaluation in ref. [10], the AlH_3 dehydrogenation had also to be included into the evaluation to get own values which use the same equipment of thermal analysis to be implemented in the evaluation of the overlapping oxidation. The kinetic data have to describe the dehydrogenation prior to the passivation. The evaluation procedure used a non-linear least-squares-fit routine of Wolfram Mathematica® "FindMinimum", describing the Thermal Analysis curves, equ. (5) – (8). The curves obtained by various heating rates were fitted simultaneously to get one kinetic data set. In addition, the DSC curves were also used together with TG curves in an additional variant. The TG data, normalized from 1 to 0, were used untreated. The DSC curves vary strongly in intensity with heating rate and the curves with high heating rates would dominate the fit procedures. Therefore the DSC curves were weighed by dividing them by their maximum, which enabled a combined fit together with TG curves. In table 1 the kinetic data are listed including the different least-squares-fit versions

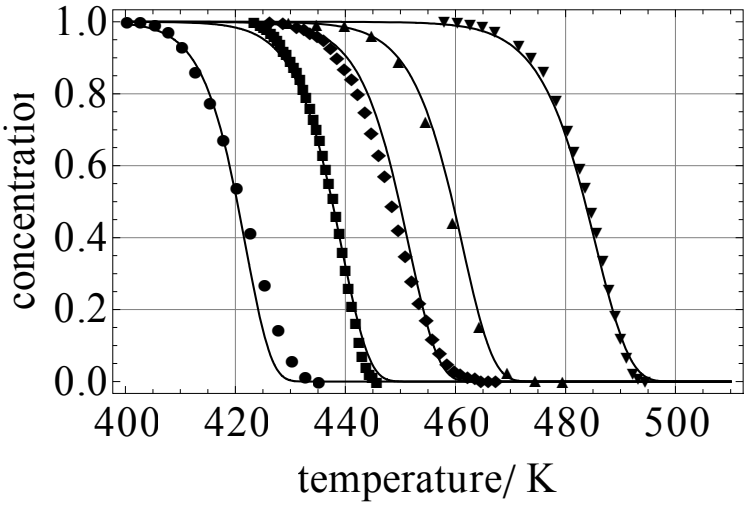

Figure 6: TG-curve dehydrogenation at heating rates 0.5, 2, 5, 10, 50 K/min: experimental data (the weight loss from 100% Alane to 90-92% resulting Al is normalized from 1 to 0 and calculated TG curves using an Avami-Erofeev model with n=2.67 (equs. (4, 5)

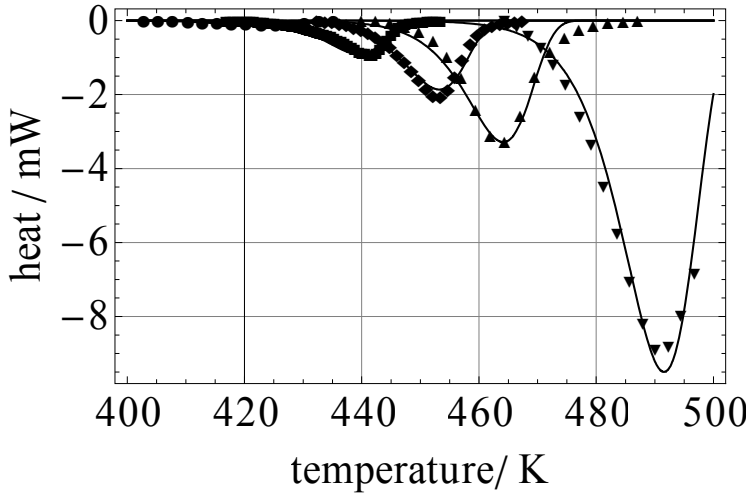

Figure 7: DSC-curve dehydrogenation at heating rates 0.5, 2, 5, 10, 50 K/min: experimental data and calculated TG curves using an Avami-Erofeev model, n=3.02 (eqs. (4 and 6)

4.1 Dehydrogenation

The E-A mechanism uses an exponent which can be related to the geometrical nucleation process of particles which can vary from less than 1 to 4 [33]. The dehydrogenation showed that only an A-E mechanism could adequately describe the curves with respect to their shape and shift according to the heating rate. The exponents were used in one version as variable and in the other as fixed with n=3. An example of a set of TG curves and DSC curves is plotted in Fig 6 and 7. For n= 3 the standard deviation σ was about 7% and for a fitted n of 2.87 about 4%. The fit of the DSC curves resulted in n=3.02 and similar standard deviations.

4.2 Oxidation (passivation reaction)

From a TG–curve measured in air (fig 3 and 5) the subtraction of a calculated (or experimental) TG-curve of dehydrogenation 100-90% (this difference normalized to 1 and 0) gives the normalized weight increase caused by the passivation. The resulting curves are fitted by a 1st order reaction and the approach is plotted in Fig. 8-9. Figure 9 shows the TG curves at heating rates of 2, 5 and 10 K/min.

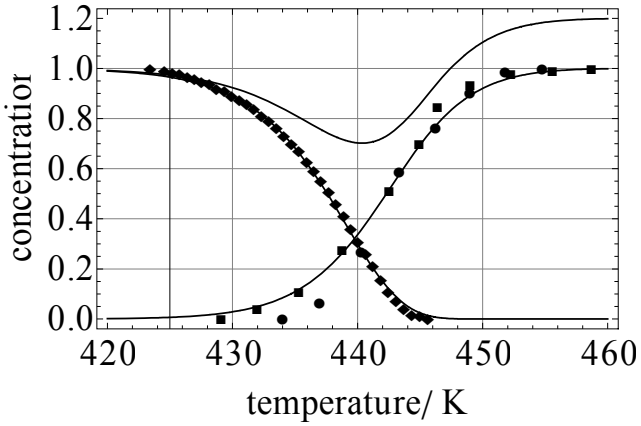

Figure 8: A TG-curve of overlapping dehydrogenation and passivation at 2 K/min (solid line above), a dehydrogenation TG curve (experimental ■ and a calculated one by an A-E-model eqs (4) ┤ which was subtracted to obtain the oxidation curve ♦●and its least squares fit by a 1st order reaction ─ (dehydrogenation and passivation curves normalized to 0-1).

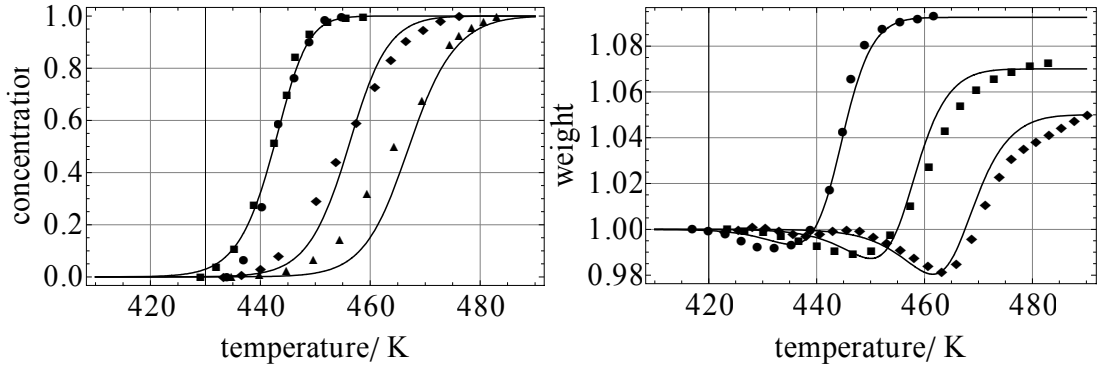

Figure 9: left hand side: TG-curves (● and ■ 2, ♦ 5, ▲10 K/min) constructed by subtracting a calculated dehydrogenation curve (A-E-model eqs (4)) from the experimental TG-curve obtained in air in the related range and a normalization to 0-1 (eqs. (4, 6)). right hand side: least squares fit of a dehydrogenation reaction overlapping with 1st order oxidation (passivation) to the experimental TG data (2 K/min,■ 5 K/min,♦10/Kmin).

Finally the calculated curves can be compared to the experimentasl ones, at least the part of the overlapping dehydrogenation and passivation. Fig. 9 compares these parts of TG-curves and shows the evaluation procedure.

The DSC curves can be directly fitted although Q_1 is small and the DSC-curve can be evaluated with the absence of the endothermic dehydrogenation. The result is shown in Fig. 10.

5.0 DISCUSSION AND CONCLUSIONS

Table 1 and 2 list the kinetic parameter obtained from the evaluation described above. The parameters of table 1were obtained from dehydration curves from TG and DSC and combining TG and DSC curves evaluation using the data weighing described above. For the E-A dehydrogenation mechanism the activation energy varies between 105 and 125 kJ/mole (see also Fig. 11) and the pre-exponential $\log_{10}Z$ between 9.9 and 12.3. This does not mean that the kinetic parameter $\log_{10}Z$ and E vary within a rectangle given by these limits. Within these limits, the kinetic parameters vary in the literature, too [10-13].

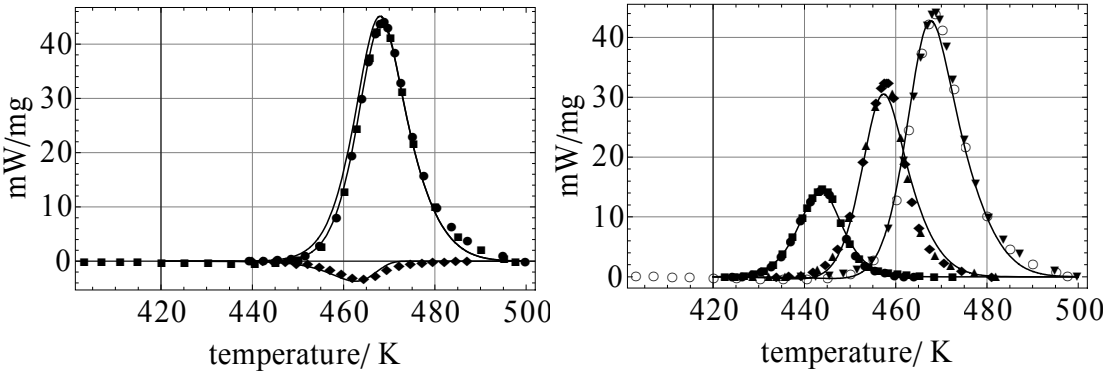

Figure 10: DSC-curve with least squares fit of an A-E-dehydrogenation reaction and a subsequent first order oxidation reaction to the experimental data for heatimng rates 2, 5 and 10K/min, left: DSC dehydrogenation, experimental curve and DSC curve only oxidation, 10K/min

In contrast, the parameters show this variation only if the following linear combination (kinetic compensation effect (see e.g. [34, 35]) is fulfilled:

$Log_{10}Z = -3.03 + 0.1224\ E$ (9)

For the oxidation reaction the linear correlation is:

$Log_{10}Z = -1.68 + 0.11123\ E$ (10)

Table 1: The kinetic parameter of the least squares fit (E-A = Avrami-Erofeev mechanism), TG curves, DSC curves were evaluated separately and combined combining also the different heating rates to obtain one data set

Method Eval.	TG E-A n=3	TG E-A n=var	TG-DSC* E-A n=3	TG-DSC* E-A n=var	TG-DSC* E-A n=3	DSC E-A n=3	DSC E-A n=var	DSC* E-A n=3	DSC* E-A n=var	DSC* E-A fit heats of reaction
E_A/k J	115.11	115.82	115.03	117.77	116.55	107.63	105.94	115.03	116.39	107.64
Log_{10} Z	11.10	11.18	11.04	11.37	11.22	10.14	9.94	11.02	11.186	10.14
n	3	2.67	3	2.58	3	3	3.02	3	2.7	3

var = variable, * for weighing DSC data were divided by the maximum value of the corresponding curve

Table 2: Kinetic data of the passivation (oxidation) 1st order reaction (for the dehydrogenation reaction an E-A-mechanism was used with n= 3, E=115.11 kJ/mole and Log Z = 11.1)

Method	TG	TG-DSC	DSC*	DSC*	TG-DSC-overall* **
E_A / kJ	93.95	83.08	83.00	82.53	67.54
Log_{10} Z	8.92	7.62	7.60	7.56	5.94

* DSC data were divided by the maximum value of the corresponding curve
** all thermo-analytical curves TG, DSC, in inert atmosphere and air at all heating rates were fitted simultaneously

A contour plot of the standard deviation depending on $log_{10}Z$ and E gives an ellipse [35] (see Fig. 10) when cut-off at $2*\sigma$, the semi major and semi minor axis of which correspond to the maximum error of the linear combination (9) and (10) of fit parameters. The minor axis is extremely small for an E-A mechanism which is related to the fact that the A-E solution for it is the power to n of a 1st order reaction TG-curve. As a result, for an E of 115.03 kJ/mole, the probable error in $Log_{10}Z$ is only 11.04±0.07 [Z - 1/s] and for $Log_{10}Z$=11.04 [Z -1/s] the possible error amounts to 115.03±1 kJ/mole on an assumed maximum error of $2*\sigma$. The passivation obviously preserves the particle sizes of the resulting Al whereas these sizes cannot be described reproducibly. Therefore, the results enable only an estimation of kinetics which is analysed by a consecutive step of a formal 1st order reaction using eq. (6) following an A-E decomposition mechanism. The estimated E amounts to about 142 kJ/mole and $log_{10}Z$ to about 13.2 [Z - 1/s]. Fig. 11 shows the growth as radii to an assumed final 1 µm crystallite. X-ray data indicate nucleation to be the rate controlling step [11, 14]. The particle radii from own x-ray measurements (TOPAS software from Siemens derives sizes as diameters) at heating rates lower than 2K/min confirms the estimated value for 2K/min because it gave radii of about 40 nm. It is unclear at what temperatures the crystal size emerges and under what conditions. The temperatures in Fig. 11 are taken from the peak maxima of the passivation DSC-curve and the error bars from the width of these peaks. The crystal size is estimated from the increase of TG-curve on passivation, which scatters strongly (see error bars of the ordinate). A radius of 0.38 nm was found for the smallest heating rate.

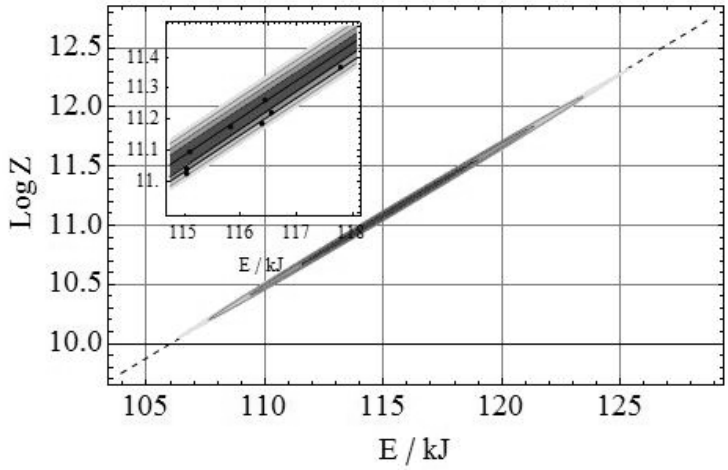

Figure 11: Kinetic compensations effect for the dehydrogenation reaction and the ensemble of kinetic parameters from the fits as dots in the inset of the graphic, the contour plot shows 2*σ (outer contour of the ellipse with extremely small minor axis) with minimum at σ, which was the relative standard deviation

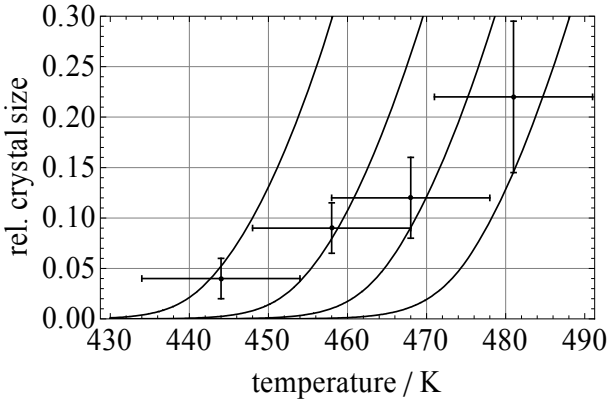

Figure 12: Estimated crystal growths depending on the heating rate 2, 5, 10 and 20 K/min

The large conversion of Al by the passivation at the lower heating rates would lead to strong heat up of the residual Al which might destroy the containment and enable a continued oxidation above 800K which converts an additional amount of about 10 nm of the particle radius in an enhanced rate compared to the subsequent diffusion controlled complete oxidation [26-28]. These further steps are also observed for the Al decomposed from AlH_3 (see Fig. 2, 3 and 4) [24, 25] and enhance the risks. The approach, to determine the kinetics of Al passivation by analysing the TG and DSC curves in an air flow, can derive kinetic parameters; in literature only a direct computation of the passivation was found [37].

REFERENCES

1. L.T. DeLuca, L. Galfetti, F. Severini, L. Rossettini, L. Meda, G. Marra, B. D'Andrea, V. Weiser, M. Calabro, A.B. Vorozhtsov, A.A. Glazunov and G.J. Pavlovets, Physical and ballistic characterization of AlH3-based space propellants, *Aerospace Sci. Tech.*, **11,** No1 2007, pp. 18-25
2. L.-T. DeLuca, L. Galfetti, F. Severini, L. Rossettini, L. Meda, G. Marra, B. D'Andrea, V. Weiser, M. Calabro, A. Vorozhtsov, A.-A. Glazunov, G.-J. Pavlovets; Physical and Ballistic Characterisation of AlH3 Based Space Propellants; European Conference for Aero-Space Science; 4-7.July, 2005; Moscow

3. T. Bazyn, R. Eyer, H. Krier and N. Glumac, Combustion characteristics of aluminum hydride at elevated pressure and temperature, *J. Propulsion and Power*, **20**, No 3, 2004, pp. 427–431
4. T. Bazyn, R. Eyer, H. Krier, N. Glumac, Dehydrogenation and burning of aluminum hydride at elevated pressures, AIAA Paper 2004-789, 2004.
5. M. Calabro, LOX/HTPB/AlH_3 hybrid propulsion for launch vehicles boosters, AIAA Paper 2004-3823, 2004.
6. M. L. Chan and C. L. Johnson, Evaluation of AlH3 for propellant application. In: L.T. DeLuca, Editor, Proceedings 8-IWCP, Grafiche GSS, Bergamo, Italy (2003) (Paper 33).
7. N. Glumac, H. Krier, T. Bazyn and R. Eyer, The combustion characteristics of aluminum hydride under solid rocket motor conditions. In: L.T. DeLuca, L. Galfetti and R.A. Pesce-Rodriguez, Ed., Proceedings 9-IWCP, Grafiche GSS, Bergamo, Italy (2004) (Paper 46).
8. A.P. Il'in, N.V. Bychin and A.A. Gromov, Products of combustion of aluminum hydride in air, *Combustion, Explosion, and Shock Waves*, **37**, No 4, 2001, pp. 231–236.
9. G.K. Lund, M.W. Lesley, J. Hanks; Characterization and Synthesis of Alpha Alane; 37th International Ann. Conference ICT, June 27-30, 2006, Karlsruhe, Germany,142-(1-11)
10. I.M.K. Ismail; T. Hawkins, Kinetics of thermal decomposition of aluminium hydride: I-non-isothermal decomposition under vacuum and in inert atmosphere (argon), *Thermochim. Acta*, **439**, 2005, pp. 32-43
11. J. Graetz., J. J. Reilly, Decomposition Kinetics of the AlH3 Polymorphs, J. *Phys. Chem. B*, **109**, No 47, 2005, pp. 22181 -22185.
12. J. Graetz., J. J. Reilly, Thermodynamics of the α, β and γ polymorphs of AlH_3, *J. Alloys Compds*, **424**, 2006, pp. 262-265
13. J. Graetz, J.J. Reilly, J.G. Kulleck and R.C. Bowman, Kinetics and thermodynamics of the aluminum hydride polymorphs, *J. Alloys Compds*., **446-447**, 2007, pp. 271-275
14. J.P. Maehlen, V.A. Yartys, R.V. Denys, M. Fichtner, Ch. Frommen, B.M. Bulychev, P. Pattison, H. Emerich, Y.E. Filinchuk, D. Chernyshov, Thermal decomposition of AlH3 studied by in situ synchrotron X-ray diffraction and thermal desorption spectroscopy, J. *Alloys Compds.*, **446-447**, 2007, pp. 280-289
15. H. Saitoh, A. Machida, Y. Katayama, K. Aoki, Formation and decomposition of AlH_3 in the aluminum-hydrogen system, *Applied Physics Letters*, **93**, No 15, 2008, pp. 151918 - 151918-3
16. M.A. Petrie, J.C. Bottaro, R.J. Schmitt, P.E. Penwell, D.C. Bomberger, Preparation of aluminum hydride polymorphs, particularly stabilized α-AlH_3, Patent No. US 6 228 338, 2001.
17. M.A. Petrie, J.C. Bottaro, R.J. Schmitt, P.E. Penwell, D.C. Bomberger, Stabilized aluminum hydride polymorphs, Patent No. US 6 617 064,
18. S. Muto, K. Tatsumi, K Ikeda, S. Orimo, Dehydrogenation process of α-AlH3 observed by transmission electron microscopy and electron energy-loss spectroscopy, *J. Applied Physics*, **105**, No 12, 2009, pp. 123514 - 123514-4
19. K. Ikeda, S. Muto, K. Tatsumi, M. Menjo1, S. Kato, M. Bielmann, A. Züttel, C. M. Jensen, S. Orimo, Dehydrogenation reaction of AlH_3: in situ microscopic observations combined with thermal and surface analyses, *Nanotechnology,* **20**, 2009, pp. 204004
20. F. M. Brower, N. E. Matzek, P. F. Reigler, H. W. Rinn, C. B. Roberts, D. L. Schmidt, J. A. Snover, K. Terada, Preparation and properties of aluminum hydride, Preparation

and properties of aluminum hydride, *J. Am. Chem. Soc*., **98**, No 9, 1976, pp 2450–2453

21. C. Sinke, L.C. Walker, F.L. Oetting and D.R. Stull, Thermodynamic properties of aluminum hydride*, J. Chem. Phys.* **47**, 1967, pp. 2759–2761
22. P. J. Herley. O. Christofferson, J. A. Todd, Microscopic observations on the thermal decomposition of α-aluminum hydride, *J. Solid State Chem.*, **35**, 1980, pp. 391
23. P. J. Herley, O. Christofferson and R. Irwin, Decomposition of .alpha.-aluminum hydride powder. 1. Thermal decomposition, *J. Phys. Chem.*, **85**, 1981, pp 1874–1881
24. N. Eisenreich, V. Weiser, A. Koleczko, E. Roth, On the Oxidation of AlH_3 as a Component to be Used in Rocket Propellants, Proceedings 3rd European Combustion Meeting ECM 2007, Crete, Greece 11-13 April 2007, pp. 17-5
25. V. Weiser, N. Eisenreich, A. Koleczko, E. Roth, On the Oxidation and Combustion of AlH3 a Potential Fuel for Rocket Propellants and Gas Generators, *Propellants, Explos., Pyrotech.*, **32**, No 3, 2007, pp. 213
26. N. Eisenreich, H. Fietzek, M. del Mar Juez-Lorenzo, V. Kolarik, A. Koleczko, V. Weiser, On the Mechanism of Low Temperature Oxidation for Aluminum Particles down to the nano-Scale, *Propellants, Explos., Pyrotech.,* **29**, 2004, pp. 137 – 145,
27. M. A. Trunov, M. Schoenitz, E. L. Dreizin, Ignition of Aluminum Powders Under Different Experimental Conditions, *Propellants, Explos., Pyrotech*., **30,** 2005, pp. 36-43
28. M. A. Trunov, S. M. Umbrajkar, M. Schoenitz, J. T. Mang, E. L. Dreizin, Oxidation and Melting of Aluminum Nanopowders, *J. Phys. Chem. B*, **110**, 2006, pp. 13094 - 13099
29. D. E. G. Jones, P. Brousseau, R. C. Fouchard, A. M. Turcotte and Q. S. M. Kwok, Thermal Characterization of Passivated Nanometer Size Aluminium Powders, *J. Thermal Anal. Cal.*, **61,** 2000, pp. 1388
30. L. P. H. Jeurgens, W. G. Sloof, F. D. Tichelaar and E. J. Mittemeijer, Structure and morphology of aluminium-oxide films formed by thermal oxidation of aluminium, *Thin Solid Films*, **418**, 2002, pp. 89-101
31. T. L. Connell Jr., G. A. Risha, R. A. Yetter, G. Young, D. S. Sundaram, V. Yang, Combustion of alane and aluminum with water for hydrogen and thermal energy generation, Proc. Combust. Inst. (2010), 33, 2, 2011, 1957-1965, doi:10.1016/j.proci.2010.07.088
32. G.V. Ivanov, F. Tepper, "Activated Aluminum as a Stored Energy Source for Propellants", Fourth International Symposium on Special Topics in Chemical Propulsion, Challenges in Propellants and Combustion 100 Years after Nobel, Stockholm, Sweden, 27-28 May, 1996.
33. V. A. Arkhipov, G.V. Ivanov, A.G. Korotkikh, V.V. Medvedev, and V. G. Surkov. Features of Ignition and Burning of Composite Propellants with Nanosized Aluminum Powder, in Burning and Gas Dynamics of Dispersion System, Materials of the 3rd International School Inter Chamber Processes, Saint Petersburg, 2000, pp.80–81.
34. S. Vyazovkin, D. Dollimore, Linear and Nonlinear Procedures in Isoconversional Computations of the Activation Energy of Nonisothermal Reactions in Solids, *J. Chem. Inf. Comput. Sci.,* **36**, 1996, pp. 42-45
35. N. Eisenreich, Direct least squares fit of chemical reaction curves and its relation to the kinetic compensation effect, *J. Thermal Anal*., **19**, 1980, pp. 289-296
36. W. H. Press, B. P. Flannery, S. A. Teukolsky, W. T. Vetterling, Numerical Recipes, 1986, Cambridge University Press, London
37. T. Campbell, R. K. Kalia, A. Nakano, P. Vashishta, S. Ogata, S. Rodgers, Dynamics of Oxidation of Aluminum Nanoclusters using Variable Charge Molecular-Dynamics Simulations on Parallel Computers, Phys. Rev. Lett.. 82, 24 (1999) 4866-4869